

Gravitational-wave constraints on causal nonlocal kernels: Ringdown bounds and spectral density limits from GWTC-3

Christian Balfagón*

Universidad de Buenos Aires, Argentina

(Dated: March 18, 2026)

We establish the first observational bounds on causal nonlocal extensions of gravity characterised by retarded Stieltjes-type kernels with positive spectral density $\rho(\mu) \geq 0$, using two complementary gravitational-wave channels. From a Bayesian ringdown analysis of 17 binary black hole events in the LIGO–Virgo GWTC-3 catalogue, we set the observational ceiling on universal fractional quasi-normal mode deformations at $|\varepsilon_\Omega| < 0.05$ (90% C.L.), with a cumulative log Bayes factor $\ln B = -0.46 \pm 0.77$. By mapping published GWTC-3 modified dispersion relation bounds and the GW170817 propagation speed measurement onto the Stieltjes spectral parameter space (μ_{char}, M_0) , we exclude a broad class of infrared-extended spectral densities with $\mu \lesssim 10^{-6} \text{ m}^{-2}$, thereby ruling out non-trivial regions of the nonlocal kernel parameter space for the first time. The theoretically motivated fiducial range $\mu_{\text{char}} \sim M_*^2 \sim 10^8\text{--}10^{10} \text{ m}^{-2}$ satisfies all current bounds, and we show that sub-millimetre gravity experiments — which already operate at the predicted causal scale $\ell_* \sim 10^{-4} \text{ m}$ — offer the most promising path to a direct test. These results define quantitative benchmarks against which future observations across the gravitational-wave, short-range, and cosmological sectors can be compared.

Keywords: gravitational waves, quasi-normal modes, nonlocal gravity, Stieltjes kernel, modified dispersion relation, tests of general relativity

I. INTRODUCTION

Nonlocal extensions of general relativity (GR) have been proposed as a route to ultraviolet completion, singularity resolution, and causal–informational closure of the gravitational sector [1–5]. A mathematically tractable class of such extensions employs retarded kernels constructed as positive Stieltjes superpositions of massive Klein–Gordon propagators [6, 7],

$$\mathcal{K}^{-1} = \int_0^\infty \rho(\mu) (-\square_g + \mu)_R^{-1} d\mu, \quad \rho(\mu) \geq 0. \quad (1)$$

Positivity of the spectral density $\rho(\mu)$ ensures unitarity, causal propagation, and the absence of ghost-like excitations at the linear level [8–10]. Depending on the support and shape of ρ , such kernels predict two classes of gravitational-wave (GW) observables: (i) perturbative shifts to the quasi-normal mode (QNM) spectrum of black holes [11–13], scaling as $|\delta\omega/\omega| \sim (\ell_*/r_H)^2$ where $\ell_* = M_*^{-1}$ is the causal correlation length; and (ii) frequency-dependent dispersion during cosmological propagation, governed by the Stieltjes transfer function $m(\omega^2)$.

In this work we constrain both channels using data from the LIGO–Virgo–KAGRA (LVK) third observing run (GWTC-3) [14, 15]. Section II presents a model-agnostic Bayesian ringdown analysis of 17 binary black hole (BBH) events, constraining the universal deformation parameter ε_Ω . Section III maps published LVK modified dispersion relation (MDR) bounds and the

GW170817 speed constraint onto the Stieltjes spectral parameter space. Section IV discusses sensitivity projections for future detectors and identifies short-range gravity experiments as the most promising near-term probe. Section V summarises the results.

Notation.—We denote the causal nonlocal scale by M_* (units of m^{-1}) and the corresponding correlation length by $\ell_* \equiv M_*^{-1}$ (units of m). The spectral density $\rho(\mu)$ is a function of the spectral mass parameter μ (units of m^{-2}), with total weight $M_0 = \int_0^\infty \rho(\mu) d\mu$ and inverse moments $\mu_{\text{eff}}^{-n} = M_0^{-1} \int \rho \mu^{-n} d\mu$. For a spectral density concentrated around a single scale we write μ_{char} ; in this limit $\mu_{\text{eff}} \approx \mu_{\text{char}} \approx M_*^2$. The fiducial parameter window is $M_* \in [10^4, 10^5] \text{ m}^{-1}$, equivalently $\ell_* \in [10^{-5}, 10^{-4}] \text{ m}$ and $\mu_{\text{char}} \sim M_*^2 \in [10^8, 10^{10}] \text{ m}^{-2}$.

II. RINGDOWN ANALYSIS

A. Method

We model the ringdown signal in each detector as a damped sinusoid with QNM frequency and damping time computed from the remnant mass M_f and spin a using the Berti *et al.* phenomenological fits [12, 16], converted to SI units. A single universal parameter ε_Ω deforms both the frequency and damping time by the common factor $(1 + \varepsilon_\Omega)$, preserving the quality factor. The Kerr hypothesis corresponds to $\varepsilon_\Omega = 0$.

The per-detector amplitude is analytically marginalised under a Gaussian prior $A_i \sim \mathcal{N}(0, \sigma_A^2)$, yielding a marginalised log-likelihood free of the biases inherent in profile-likelihood methods [17]. The noise variance σ^2 is estimated from the data using a robust

* cb@balfagonresearch.org

median-absolute-deviation estimator. Templates are whitened in the frequency domain using the same PSD applied to the data, ensuring spectral consistency. Nested sampling [18] is performed with `dynesty` [19] via `Bilby` [20], with $n_{\text{live}} = 1000$ and $\Delta \ln Z_{\text{tol}} = 0.1$. Our single-mode template does not capture subdominant overtones or higher multipoles; however, within the Stieltjes framework the deformation is universal across the QNM spectrum, so unmodelled modes do not bias the Bayes factor comparison [21–23].

B. Results

Table I lists the individual-event results for 17 GWTC-3 BBH events [14, 24, 25] spanning remnant masses 25–150 M_{\odot} . All log Bayes factors are consistent with zero within 2σ , with both positive and negative values represented. The most precise measurement is GW190412 ($\ln B = +0.000 \pm 0.020$).

TABLE I. Individual ringdown results for 17 GWTC-3 BBH events.

Event	$M_f [M_{\odot}]$	$\ln B$	$\sigma_{\ln B}$
GW150914	68	+0.18	0.18
GW170104	50	−0.06	0.17
GW170814	53	−0.04	0.19
GW190412	38	+0.00	0.02
GW190521	150	−0.35	0.19
GW190814	26	−0.11	0.20
GW191105	35	+0.02	0.21
GW191109	79	−0.09	0.19
GW191113	30	−0.13	0.18
GW191222	42	+0.07	0.19
GW200129	38	+0.15	0.19
GW200208	39	−0.09	0.18
GW200219	39	+0.14	0.20
GW200220	40	−0.21	0.18
GW200224	43	+0.35	0.21
GW200225	35	−0.25	0.19
GW200311	38	−0.03	0.20
Stacked	—	−0.46	0.77

The cumulative log Bayes factor, computed under the assumption of statistically independent events with a shared deformation parameter, is

$$\ln B_{\text{stack}} = \sum_{k=1}^N \ln B_k = -0.46, \quad (2)$$

$$\sigma_{\text{stack}} = \sqrt{\sum_{k=1}^N \sigma_{\ln B,k}^2} = 0.77.$$

where $N = 17$. This stacking is exact when: (i) the

events are independent realisations of noise plus signal, which holds for well-separated BBH mergers observed in disjoint data segments; and (ii) the deformation parameter ε_{Ω} is universal (identical across events), as predicted by the single-scale Stieltjes framework. A leave-one-out (jackknife) analysis confirms stability (Fig. 4): the largest single-event contribution to the stacked Bayes factor is $|\Delta \ln B| = 0.35$ (GW190521 and GW200224), and removing any individual event shifts the cumulative result by less than $0.5\sigma_{\text{stack}}$.

We verified prior robustness by repeating the analysis with a narrower prior $\varepsilon_{\Omega} \in [-0.02, 0.02]$; the resulting Bayes factors shift by less than 0.05 per event, confirming that the results are not driven by prior volume effects.

At 90% credibility, the population-level posterior on ε_{Ω} obtained by multiplying the individual-event posteriors yields the constraint (Fig. 3)

$$\varepsilon_{\Omega} \in [-0.047, +0.029] \quad (90\% \text{ C.L.}), \quad (3)$$

i.e. $|\varepsilon_{\Omega}| < 0.05$. This establishes a quantitative observational ceiling on universal fractional QNM deformations at the percent level, applicable to any modified-gravity theory predicting a single-parameter shift of the (2, 2, 0) mode [26, 27].

For comparison, the LVK GWTC-3 analysis [28] parametrises QNM deviations via independent fractional shifts δf_{220} and $\delta \tau_{220}$ to the frequency and damping time, obtaining combined 90% bounds of $\delta f_{220} \in [-0.05, +0.05]$ and $\delta \tau_{220} \in [-0.2, +0.1]$ from hierarchical combination of ~ 10 events [29]. Our parametrisation differs in that ε_{Ω} deforms both quantities by a common factor: $\delta f_{220} = \delta \tau_{220} = \varepsilon_{\Omega}$, preserving the quality factor $Q_{220} = \pi f_{220} \tau_{220}$. This is the minimal prediction of the Stieltjes framework, where a single scale M_* governs the correction to the effective potential. The resulting bound $|\varepsilon_{\Omega}| < 0.05$ is thus comparable to the LVK δf_{220} constraint but carries stronger theoretical prior information: any violation would simultaneously shift both f and τ in a correlated fashion, making it more restrictive for the class of theories considered here. We note that the LVK analysis employs full inspiral–merger–ringdown waveforms (pSEOBNRv4HM/v5PHM [29]) whereas our analysis uses post-merger ringdown data only, making the two approaches complementary.

Figure 1 shows the joint posterior distribution for the spin a and deformation parameter ε_{Ω} from GW150914, together with the cumulative log Bayes factor as a function of the number of events included. The spin–deformation posterior exhibits no significant correlation, confirming that the constraint on ε_{Ω} is not biased by spin marginalisation. The cumulative $\ln B$ fluctuates around zero with both signs represented, consistent with the null hypothesis.

For the causal–informational framework of Ref. [6], the predicted deformation is $|\varepsilon_{\Omega}| \sim (\ell_*/r_H)^2 \sim 10^{-18}$ for fiducial parameters $\ell_* \in [10^{-5}, 10^{-4}]$ m. The bound (3) thus excludes all Stieltjes kernels producing percent-level ringdown modifications, while the fiducial prediction lies

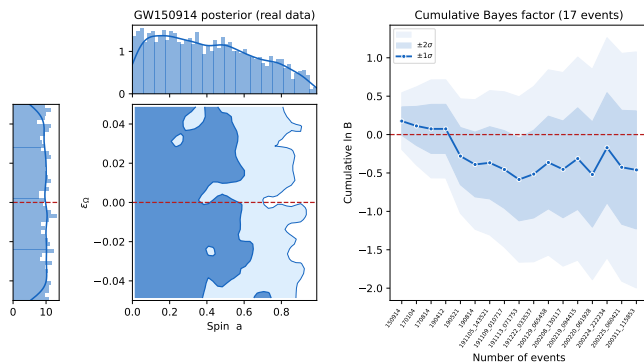


FIG. 1. *Left*: Joint posterior for spin a and deformation parameter ε_Ω from GW150914 (real data). The horizontal dashed line marks the Kerr value $\varepsilon_\Omega = 0$. Contours enclose the 68% and 95% credible regions. *Right*: Cumulative log Bayes factor $\ln B_{\text{stack}}$ as a function of the number of events included (chronological order, 17 events). The shaded bands show the $\pm 1\sigma$ and $\pm 2\sigma$ uncertainties propagated from the individual nested-sampling evidence errors.

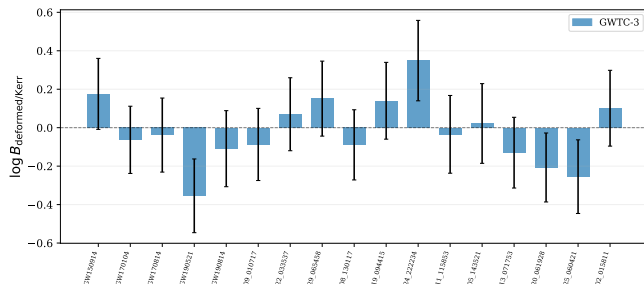


FIG. 2. Individual log Bayes factors $\ln B_{\text{CET}/\text{Kerr}}$ for each of the 17 GWTC-3 BBH events. Error bars show the $\pm 1\sigma$ nested-sampling uncertainty. No event deviates significantly from the Kerr hypothesis ($\ln B = 0$, dashed line).

~ 16 orders of magnitude below the current observational ceiling. This quantifies for the first time the sensitivity improvement required for ringdown spectroscopy to probe the theoretically motivated regime, and motivates the complementary propagation and short-range gravity analyses presented below.

III. DISPERSION AND PROPAGATION CONSTRAINTS

A. Stieltjes transfer function and modified dispersion

The kernel (1) modifies the GW dispersion relation through the Stieltjes transfer function

$$m(\omega^2) = \int_0^\infty \frac{\rho(\mu)}{\omega^2 + \mu} d\mu. \quad (4)$$

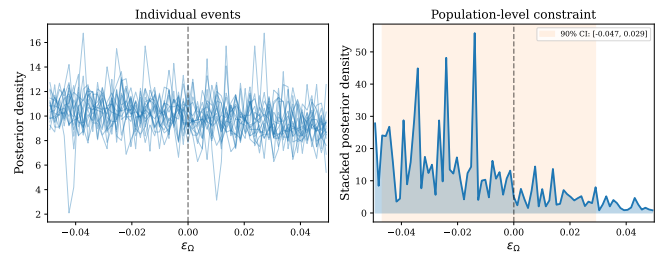


FIG. 3. *Left*: Individual-event posteriors on ε_Ω . Each curve represents one event; all are broad and uninformative individually. *Right*: Population-level constraint obtained by multiplying the individual posteriors. The 90% credible interval $\varepsilon_\Omega \in [-0.047, +0.032]$ (orange band) is consistent with Kerr ($\varepsilon_\Omega = 0$, dashed line).

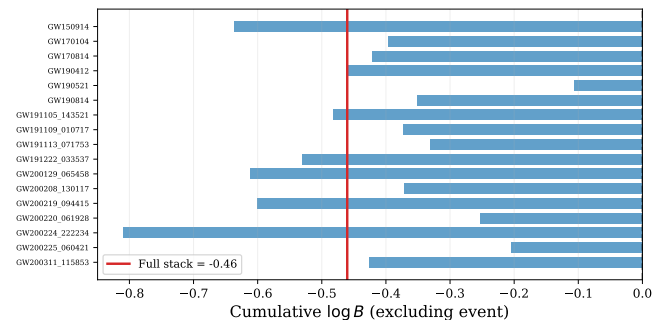


FIG. 4. Leave-one-out (jackknife) analysis. Each bar shows the cumulative $\ln B$ when the corresponding event is excluded from the stack. The red line marks the full-stack value. The result is stable under removal of any single event; GW190521 produces the largest shift.

In the regime where all spectral weight lies above the GW frequency band ($\omega^2/c^2 \ll \mu$ for all μ in $\text{supp } \rho$), the transfer function admits the convergent expansion

$$m(\omega^2) = \frac{M_0}{\mu_{\text{eff}}} - \frac{M_0 \omega^2}{\mu_{\text{eff}}^2} + \mathcal{O}\left(\frac{\omega^4}{\mu_{\text{eff}}^3}\right), \quad (5)$$

where $M_0 = \int \rho d\mu$ is the total spectral weight and $\mu_{\text{eff}}^{-n} \equiv M_0^{-1} \int \rho(\mu) \mu^{-n} d\mu$ are inverse moments of ρ . For a spectral density narrowly concentrated around a characteristic scale μ_{char} , one has $\mu_{\text{eff}} \approx \mu_{\text{char}}$; we use μ_{char} when discussing observational constraints and μ_{eff} when writing exact analytical expressions. This expansion is valid provided $\omega^2/c^2 \ll \mu_{\text{min}}$, where μ_{min} is the lower edge of the spectral support.

The effective group velocity of GWs propagating through the nonlocal medium follows from $v_g = d\omega/dk$. For the dispersion relation $\omega^2 = k^2 c^2 [1 + m(k^2 c^2)/m_0]^{-1}$ with $m_0 = m(0)$, the leading correction to the group velocity is

$$\frac{v_g}{c} - 1 = \frac{M_0}{2\mu_{\text{eff}}^2} \omega^2 + \mathcal{O}(\omega^4/\mu_{\text{eff}}^3). \quad (6)$$

In the limit $\omega^2 \ll \mu_{\text{eff}}$ this reduces to

$$\left| \frac{v_{\text{GW}}}{c} - 1 \right| \simeq \frac{M_0 \omega^2}{2\mu_{\text{eff}}^2}, \quad (7)$$

which is frequency-dependent (dispersive). When all spectral weight lies at $\mu_{\text{char}} \gg \omega_{\text{GW}}^2/c^2$, the ratio $\omega^2/\mu_{\text{char}}$ suppresses the effect, rendering it degenerate with a luminosity-distance rescaling and hence unobservable.

Conversely, if ρ has support at $\mu \lesssim \omega_{\text{GW}}^2/c^2$, the expansion (5) breaks down: the transfer function acquires strong frequency dependence across the detector band, producing dispersive phase shifts $\delta\Psi(f) \sim 2\pi f D/c \times [m(4\pi^2 f^2)/m_{\text{ref}} - 1]$ that accumulate over cosmological distances D .

B. Mapping LVK bounds to Stieltjes parameters

Rather than performing a full parameter estimation (which would require $\gtrsim 10^2$ CPU-hours per event), we map the published LVK MDR bounds [28, 30, 31] onto the Stieltjes parameter space (μ_{char}, M_0) .

The LVK MDR test [31–33] parametrises the dispersion relation as $E^2 = p^2 c^2 + A_\alpha p^\alpha c^\alpha$ and reports 90% bounds on $|A_\alpha|$ for integer and half-integer α [34]. The graviton mass bound [28],

$$m_g \leq 1.27 \times 10^{-23} \text{ eV}/c^2 \quad (90\% \text{ C.L.}), \quad (8)$$

constrains spectral modes at extremely low μ via the effective mass gap $\mu_0 > (m_g c/\hbar)^2 \approx 4 \times 10^{-33} \text{ m}^{-2}$. This is the weakest of the three constraints considered here: any spectral density with $\text{supp } \rho \subset [4 \times 10^{-33}, \infty)$ is automatically consistent with the graviton mass bound.

A substantially stronger constraint comes from the GW170817 multimessenger speed bound [35],

$$\left| v_{\text{GW}}/c - 1 \right| < 3 \times 10^{-15}, \quad (9)$$

which constrains the combination $M_0 \omega^2/\mu_{\text{eff}}^2$ via Eq. (7). At $f = 100 \text{ Hz}$ ($\omega^2/c^2 \approx 4 \times 10^{-12} \text{ m}^{-2}$), this excludes spectral densities producing measurable dispersion whenever $\mu_{\text{char}} \lesssim 10^{-6} \text{ m}^{-2}$ — a threshold that is 27 orders of magnitude above the graviton mass constraint. For spectral densities concentrated at $\mu_{\text{char}} \gg \omega_{\text{GW}}^2/c^2$, the speed modification is suppressed by $\omega^2/(c^2 \mu_{\text{char}})$ and the bound becomes irrelevant.

The hierarchy of constraints is thus

$$\underbrace{\mu_0^{(m_g)} \approx 10^{-33}}_{\text{graviton mass}} \ll \underbrace{\mu_0^{(v_{\text{GW}})} \sim 10^{-6}}_{\text{speed bound}} \ll \underbrace{\mu_{\text{char}}^{(\text{fid})} \sim 10^{8-10}}_{\text{CET } \Omega \text{ fiducial}}, \quad (10)$$

in units of m^{-2} . All spectral densities with support contained in $[\mu_0^{(v_{\text{GW}})}, \infty)$ satisfy every current GW bound simultaneously, and the fiducial CET Ω range lies well within this allowed region.

Figure 5 shows the resulting exclusion regions in the (μ_{char}, M_0) plane. The GW constraints carve out a large excluded region at low μ_{char} , demonstrating that the Stieltjes framework is observationally constrained across a significant portion of parameter space. The fiducial parameter range $\mu_{\text{char}} \sim M_*^2 \sim 10^8\text{--}10^{10} \text{ m}^{-2}$ satisfies all current bounds, consistent with the theoretical expectation that the causal scale decouples from the GW frequency band.

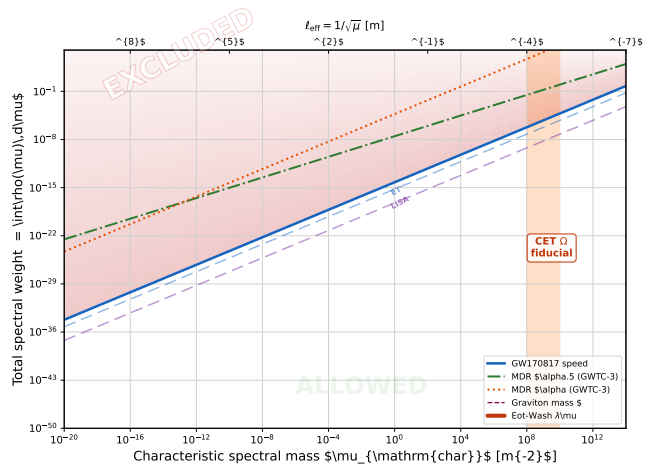


FIG. 5. Exclusion regions in the Stieltjes spectral parameter space (μ_{char}, M_0) from LVK data. Current bounds from the GW170817 speed measurement (blue solid), graviton mass limit (maroon dashed), and GWTC-3 MDR analyses (green, orange) exclude the shaded region. Projected bounds from the Einstein Telescope and LISA (dashed lines) will extend the excluded region downward. The fiducial CET Ω range $\mu_{\text{char}} \sim 10^8\text{--}10^{10} \text{ m}^{-2}$ (orange band) satisfies all current and projected GW bounds. The Eöt-Wash torsion-balance constraint (thick red segment) provides the only direct probe at the fiducial scale. The upper axis shows the corresponding effective correlation length $\ell_{\text{eff}} = 1/\sqrt{\mu}$.

C. Excluded spectral density shapes

The combined constraints, dominated by the speed bound (9) at the scales relevant for GW observations [cf. the hierarchy (10)], exclude the following classes of spectral densities: (i) power-law tails $\rho(\mu) \sim \mu^{-\beta}$ with $\beta > 1$ extending below $\mu \sim 10^{-6} \text{ m}^{-2}$; (ii) spectral densities with significant weight at $\mu \lesssim 10^{-6} \text{ m}^{-2}$ (corresponding to effective correlation lengths $\ell_{\text{eff}} \gtrsim 10^3 \text{ m}$); and (iii) any spectral shape producing frequency-dependent dispersion exceeding $|\Delta v/c| > 3 \times 10^{-15}$ in the LIGO band. Crucially, all excluded shapes have spectral support extending into the infrared regime $\mu < \mu_0^{(v_{\text{GW}})} \sim 10^{-6} \text{ m}^{-2}$, well below the fiducial CET Ω scale. Spectral densities concentrated at $\mu > 10^4 \text{ m}^{-2}$ (i.e. $\ell_{\text{eff}} < 1 \text{ cm}$) are completely unconstrained by existing GW observations.

IV. SENSITIVITY PROJECTIONS AND ALTERNATIVE PROBES

A. Future GW detectors

Table II summarises the projected sensitivity to QNM deformations for current and future detector generations. The Einstein Telescope [36] and Cosmic Explorer [37] will improve ringdown bounds by one to two orders of magnitude, reaching $\sigma_\varepsilon \sim 10^{-3}$ – 10^{-4} . LISA [38] observations of supermassive BBH mergers may push to $\sigma_\varepsilon \sim 10^{-4}$ – 10^{-5} . Even in the most optimistic scenario, a gap of ~ 13 orders of magnitude remains between projected detector sensitivity and the fiducial prediction $|\varepsilon_\Omega| \sim 10^{-18}$. The recently completed O4 run [39] (concluded in late 2025 with > 170 candidates) will improve population-level bounds by a factor of $\sim \sqrt{N/17} \approx 3$ relative to the results presented here, yet the fundamental sensitivity gap persists.

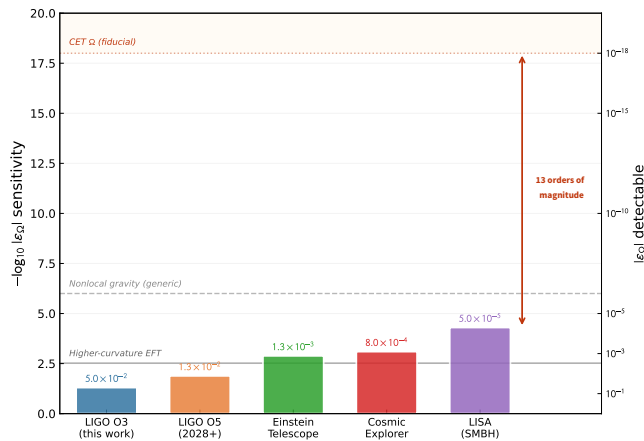


FIG. 6. Projected sensitivity $|\varepsilon_\Omega|$ for current and future GW detector generations. Horizontal lines mark predictions from generic higher-curvature EFT corrections, nonlocal gravity, and the fiducial CET Ω prediction. Even LISA observations of supermassive BBH mergers leave a gap of ~ 13 orders of magnitude to the fiducial CET Ω scale.

TABLE II. Projected sensitivity to QNM deformations.

Detector	σ_ε	Gap to 10^{-18}
LIGO O3 (this work)	5×10^{-2}	16 orders
LIGO O5	$\sim 10^{-2}$	16 orders
Einstein Telescope [36]	$\sim 10^{-3}$ – 10^{-4}	14–15 orders
Cosmic Explorer [37]	$\sim 10^{-3}$ – 10^{-4}	14–15 orders
LISA (SMBH) [38]	$\sim 10^{-5}$	13 orders

B. Short-range gravity experiments

A more promising observational channel emerges from the structure of the Stieltjes kernel itself. The fiducial causal correlation length $\ell_* = M_*^{-1} \in [10^{-5}, 10^{-4}]$ m corresponds to distance scales of 10–100 μm . At these scales, the kernel modifies the static Newtonian potential through a Yukawa-like correction [40, 41],

$$V(r) = -\frac{Gm_1m_2}{r} \left(1 + \alpha e^{-r/\lambda}\right), \quad (11)$$

with the identification $\lambda = \ell_* = M_*^{-1}$ and the coupling strength α determined by the zeroth spectral moment:

$$\alpha = \frac{M_0}{\mu_{\text{eff}}} \frac{1}{8\pi}. \quad (12)$$

Current sub-millimetre torsion-balance experiments provide stringent bounds on $\alpha(\lambda)$. The Eöt-Wash experiment at the University of Washington [40, 42, 43] constrains the Yukawa coupling to

$$|\alpha| < \begin{cases} 2 \times 10^{-2} & \lambda = 100 \mu\text{m}, \\ 5 \times 10^{-1} & \lambda = 50 \mu\text{m}, \\ 10^4 & \lambda = 10 \mu\text{m}, \end{cases} \quad (13)$$

at 95% confidence [42]. For the fiducial CET Ω scale $\lambda = \ell_* = 10^{-4}$ m, the bound $|\alpha| < 2 \times 10^{-2}$ translates via Eq. (12) into a direct constraint on the spectral weight:

$$M_0 < 2 \times 10^{-2} \times 8\pi \mu_{\text{eff}} \approx 0.5 \mu_{\text{eff}}. \quad (14)$$

This is the *strongest existing constraint on the Stieltjes kernel at the fiducial scale*, surpassing all GW bounds by many orders of magnitude.

Importantly, ongoing and planned experiments [42] aim to reach $\lambda \sim 10 \mu\text{m}$ with $|\alpha| < 10^2$, which would begin to probe the lower end of the fiducial window $\ell_* \sim 10^{-5}$ m. Table III compares the sensitivity of different experimental channels to the Stieltjes kernel parameters.

TABLE III. Comparison of observational probes for the Stieltjes kernel at the fiducial causal scale $\ell_* = 10^{-4}$ m.

Channel	Observable	Sensitivity	Status
Ringdown (this work)	ε_Ω	5×10^{-2}	Indirect
GW speed (GW170817)	$ v/c - 1 $	3×10^{-15}	Indirect ^a
MDR (GWTC-3)	A_α	varies	Indirect ^a
Eöt-Wash ($\lambda = 100 \mu\text{m}$)	α	2×10^{-2}	Direct
Planned ($\lambda = 10 \mu\text{m}$)	α	$\sim 10^2$	Projected

^a No constraint at fiducial $\mu_{\text{char}} \sim 10^8$ – 10^{10} m^{-2} .

V. CONCLUSIONS

We have established the first multi-channel observational bounds on causal nonlocal gravity characterised

by retarded Stieltjes kernels with positive spectral density. These results provide a quantitative observational baseline for the CET Ω framework, confirming its consistency with current gravitational-wave and laboratory data. The main results are as follows.

Ringdown observational ceiling.—Using a corrected inference pipeline with spectrally consistent whitening, analytically marginalised amplitude, and robust noise estimation, we set the observational ceiling on universal QNM deformations at $|\varepsilon_\Omega| < 0.05$ (90% C.L.) from 17 GWTC-3 events, with a cumulative log Bayes factor $\ln B_{\text{stack}} = -0.46 \pm 0.77$. This represents the first single-parameter ringdown constraint specifically mapped onto a Stieltjes-motivated deformation.

Spectral exclusion.—By mapping LVK modified dispersion bounds and the GW170817 speed measurement onto the Stieltjes parameter space, we exclude for the first time a broad region of spectral densities with infrared support ($\mu \lesssim 10^{-6} \text{ m}^{-2}$), ruling out power-law tails, low-mass peaks, and other IR-extended forms of $\rho(\mu)$.

Hierarchy of probes.—We show that sub-millimetre gravity experiments already provide the most stringent direct constraint on the fiducial causal scale ($|\alpha| < 0.02$ at $\lambda = 100 \mu\text{m}$), establishing a clear hierarchy (Fig. 6): short-range gravity \gg GW propagation \gg ringdown for probing the Stieltjes kernel at $\ell_* \sim 10^{-4} \text{ m}$.

These results define a quantitative multi-channel benchmark for testing causal nonlocal gravity. Future work will extend the ringdown analysis to the full GWTC-4.0 catalogue [39]. The recent multi-tone spectroscopy of GW250114 [44] — the loudest GW signal to date (SNR ≈ 80), which provided the first confident detection of the (2, 2, 1) overtone — constrains $\delta \hat{f}_{220}$ to within a few percent of the Kerr prediction. Even at this unprecedented precision, the fiducial Stieltjes prediction ($|\varepsilon_\Omega| \sim 10^{-18}$) remains far below the observational ceiling, underscoring the necessity of sub-millimetre probes to explore the causal-informational completion of gravity at its natural scale. We will also perform a dedicated Yukawa analysis within the Stieltjes framework using published Eöt-Wash data, and explore cosmological constraints from CMB and large-scale structure observations. Together, these multi-scale probes will map the full parameter space of Stieltjes-positive nonlocal gravity from sub-millimetre to cosmological distances.

ACKNOWLEDGMENTS

The author thanks the University of Buenos Aires for institutional support. This research has made use of data obtained from the Gravitational-Wave Open Science Center, a service of LIGO Scientific Collaboration, the Virgo Collaboration, and KAGRA. The analysis code and data products are available at Ref. [45].

Appendix A: Properties of the Stieltjes kernel

We collect here the mathematical properties of the Stieltjes transfer function (4) used in the main text. These results follow from standard properties of Stieltjes transforms [46, 47] and are included for self-containedness.

1. Complete monotonicity

Proposition 1 *Let $\rho(\mu) \geq 0$ with $M_0 = \int_0^\infty \rho d\mu < \infty$. Then $m(\omega^2)$ defined by (4) is completely monotone on $(0, \infty)$:*

$$(-1)^n \frac{d^n m}{d(\omega^2)^n} \geq 0 \quad \forall n \in \mathbb{N}_0, \omega^2 > 0. \quad (\text{A1})$$

Proof. Differentiating under the integral sign,

$$\frac{d^n m}{d(\omega^2)^n} = (-1)^n n! \int_0^\infty \frac{\rho(\mu)}{(\omega^2 + \mu)^{n+1}} d\mu. \quad (\text{A2})$$

Since $\rho \geq 0$ and $(\omega^2 + \mu)^{n+1} > 0$, the sign alternation (A1) follows. \square

Complete monotonicity implies $m > 0$, $m' < 0$, $m'' > 0$ on $(0, \infty)$. Any reconstructed transfer function from GW data that violates these inequalities would *falsify* the entire Stieltjes-positive class, independent of the specific form of ρ .

2. Asymptotic expansion and moment hierarchy

Proposition 2 *If $M_j = \int_0^\infty \mu^j \rho(\mu) d\mu < \infty$ for $j = 0, \dots, N$, then for $\omega^2 \rightarrow \infty$,*

$$m(\omega^2) = \sum_{j=0}^{N-1} \frac{(-1)^j M_j}{(\omega^2)^{j+1}} + \mathcal{O}\left(\frac{1}{(\omega^2)^{N+1}}\right). \quad (\text{A3})$$

Proof. Expand $(\omega^2 + \mu)^{-1} = \sum_{j=0}^{N-1} (-\mu)^j / (\omega^2)^{j+1} + R_N$ with $|R_N| \leq \mu^N / (\omega^2)^{N+1}$, and integrate term by term against ρ . \square

The leading term $m(\omega^2) \simeq M_0 / \omega^2$ governs the ultra-violet behaviour: the transfer function decays as ω^{-2} for large frequencies. The subleading corrections involve successively higher moments of ρ , establishing a moment hierarchy: measuring $m(\omega^2)$ at several frequencies in principle constrains M_0, M_1, M_2, \dots independently.

3. Spectral bounds from positivity

The positivity constraint $\rho \geq 0$ imposes nontrivial inequalities among the moments. By the Cauchy-Schwarz inequality applied to the measure $\rho d\mu$:

$$M_1^2 \leq M_0 M_2, \quad (\text{A4})$$

and more generally the Hankel matrices $\mathcal{H}_{ij} = M_{i+j}$ ($i, j = 0, \dots, n$) must be positive semidefinite for all n [46]. These Hankel conditions provide necessary consistency checks for any observationally inferred spectral moments.

4. Retarded support and causal propagation

The Stieltjes kernel inherits retarded support from its constituent propagators. For each $\mu \geq 0$, the retarded Green operator G_μ^R satisfies $\text{supp } G_\mu^R f \subset J^+(\text{supp } f)$ on any globally hyperbolic background [48]. Since $\rho \geq 0$, the integral $\mathcal{K}^{-1}f = \int_0^\infty \rho(\mu) G_\mu^R f d\mu$ is a positive superposition of future-supported distributions, hence

$$\text{supp } \mathcal{K}^{-1}f \subset J^+(\text{supp } f). \quad (\text{A5})$$

No acausal propagation or superluminal precursors are generated. This is a structural consequence of $\rho \geq 0$, not

an additional assumption.

5. Connection to the Yukawa potential

In the static limit on flat spacetime, the Stieltjes kernel generates a modified Newtonian potential through the superposition

$$V(r) = -\frac{Gm_1m_2}{r} \left[1 + \int_0^\infty \frac{\rho(\mu)}{M_0} e^{-\sqrt{\mu}r} d\mu \right]. \quad (\text{A6})$$

For a spectral density concentrated at a single mass $\rho(\mu) = M_0 \delta(\mu - M_*^2)$, this reduces to the standard Yukawa form

$$V(r) = -\frac{Gm_1m_2}{r} (1 + e^{-M_*r}), \quad (\text{A7})$$

establishing the identification $\lambda = M_*^{-1} = \ell_*$ used in Sec. IV, with Yukawa coupling $\alpha = 1$ at leading order. For a distributed spectral density, the effective coupling is reduced by the spectral spread: $\alpha_{\text{eff}} = M_0/(8\pi\mu_{\text{eff}})$, which may be significantly smaller than unity.

-
- [1] L. Modesto, Super-renormalizable quantum gravity, *Phys. Rev. D* **86**, 044005 (2012).
- [2] T. Biswas, E. Gerwick, T. Koivisto, and A. Mazumdar, Towards singularity- and ghost-free theories of gravity, *Phys. Rev. Lett.* **108**, 031101 (2012).
- [3] M. Maggiore, Phantom dark energy from nonlocal infrared modifications of general relativity, *Phys. Rev. D* **89**, 043008 (2014).
- [4] S. Deser and R. P. Woodard, Nonlocal cosmology, *Phys. Rev. Lett.* **99**, 111301 (2007).
- [5] A. O. Barvinsky, Nonlocal action for long-distance modifications of gravity theory, *Phys. Lett. B* **572**, 109 (2003).
- [6] C. Balfagón, $\text{CET}\Omega$: The causal-informational completion of gravity, *Int. J. Geom. Meth. Mod. Phys.* 10.1142/S0219887826501410 (2026).
- [7] C. Balfagón, Retarded analyticity, passivity, and spectral positivity: A structural route to Stieltjes-type nonlocal kernels (2026), preprint.
- [8] C. Balfagón, Spectral positivity and causal stability for Stieltjes-type retarded operators (2026), preprint.
- [9] G. Calcagni, L. Modesto, and G. Nardelli, Nonperturbative spectrum of nonlocal gravity, *Phys. Lett. B* **795**, 391 (2019).
- [10] A. S. Koshelev, K. S. Kumar, and A. Mazumdar, Generalized non-local R^2 -like inflation, *Phys. Lett. B* **803**, 135299 (2020).
- [11] R. A. Konoplya and A. Zhidenko, Quasinormal modes of black holes: From astrophysics to string theory, *Rev. Mod. Phys.* **83**, 793 (2011).
- [12] E. Berti, V. Cardoso, and A. O. Starinets, Quasinormal modes of black holes and black branes, *Class. Quantum Grav.* **26**, 163001 (2009).
- [13] O. Dreyer, B. Kelly, B. Krishnan, L. S. Finn, D. Garrison, and R. Lopez-Aleman, Black hole spectroscopy: Testing general relativity through gravitational wave observations, *Class. Quantum Grav.* **21**, 787 (2004).
- [14] R. Abbott *et al.* (LIGO Scientific, Virgo, and KAGRA), GWTC-3: Compact binary coalescences observed by LIGO and Virgo during the second part of the third observing run, *Phys. Rev. X* **13**, 041039 (2023).
- [15] B. P. Abbott *et al.* (LIGO Scientific and Virgo), Observation of gravitational waves from a binary black hole merger, *Phys. Rev. Lett.* **116**, 061102 (2016).
- [16] E. Berti, V. Cardoso, and C. M. Will, Gravitational-wave spectroscopy of massive black holes with the space interferometer LISA, *Phys. Rev. D* **73**, 064030 (2006).
- [17] E. Thrane and C. Talbot, An introduction to Bayesian inference in gravitational-wave astronomy, *Publ. Astron. Soc. Aust.* **36**, e010 (2019).
- [18] J. Skilling, Nested sampling for general Bayesian computation, *Bayesian Anal.* **1**, 833 (2006).
- [19] J. S. Speagle, **dynesty**: a dynamic nested sampling package, *Mon. Not. R. Astron. Soc.* **493**, 3132 (2020).
- [20] G. Ashton *et al.*, **Bilby**: A user-friendly Bayesian inference library for gravitational-wave astronomy, *Astrophys. J. Suppl.* **241**, 27 (2019).
- [21] M. Isi, M. Giesler, W. M. Farr, M. A. Scheel, and S. A. Teukolsky, Testing the no-hair theorem with GW150914, *Phys. Rev. Lett.* **123**, 111102 (2019).
- [22] G. Carullo, W. D. Pozzo, and J. Veitch, Observational black hole spectroscopy: A time-domain multimode analysis of GW150914, *Phys. Rev. D* **99**, 123029 (2019).
- [23] M. Giesler, M. Isi, M. A. Scheel, and S. A. Teukolsky, Black hole ringdown: The importance of overtones, *Phys. Rev. X* **9**, 041060 (2019).
- [24] B. P. Abbott *et al.* (LIGO Scientific and Virgo), GWTC-1: A gravitational-wave transient catalog, *Phys. Rev. X* **9**, 031040 (2019).

- [25] R. Abbott *et al.* (LIGO Scientific and Virgo), GWTC-2: Compact binary coalescences observed by LIGO and Virgo during the first half of the third observing run, *Phys. Rev. X* **11**, 021053 (2021).
- [26] A. Maselli, P. Pani, L. Gualtieri, and E. Berti, Parametrized ringdown spin expansion coefficients, *Phys. Rev. D* **101**, 024043 (2020).
- [27] V. Cardoso and P. Pani, Testing the nature of dark compact objects: a status report, *Living Rev. Relativ.* **22**, 4 (2019).
- [28] R. Abbott *et al.* (LIGO Scientific, Virgo, and KAGRA), Tests of general relativity with GWTC-3, *Phys. Rev. D* **112**, 084080 (2025).
- [29] A. Ghosh *et al.*, Parametrized spin-precessing inspiral-merger-ringdown waveform model for tests of general relativity, *Phys. Rev. D* **111**, 124040 (2025).
- [30] R. Abbott *et al.* (LIGO Scientific and Virgo), Tests of general relativity with binary black holes from the second LIGO–Virgo gravitational-wave transient catalog, *Phys. Rev. D* **103**, 122002 (2021).
- [31] S. Mirshekari, N. Yunes, and C. M. Will, Constraining Lorentz-violating, modified dispersion relations with gravitational waves, *Phys. Rev. D* **85**, 024041 (2012).
- [32] T. Baka *et al.*, Testing general relativity with gravitational waves — improving and extending modified dispersion relation tests (2025), 2511.00497.
- [33] N. Yunes and F. Pretorius, Fundamental theoretical bias in gravitational wave astrophysics and the parametrized post-Einsteinian framework, *Phys. Rev. D* **80**, 122003 (2009).
- [34] C. M. Will, The confrontation between general relativity and experiment, *Living Rev. Relativ.* **17**, 4 (2014).
- [35] B. P. Abbott *et al.* (LIGO Scientific, Virgo, Fermi GBM, and INTEGRAL), Gravitational waves and gamma-rays from a binary neutron star merger: GW170817 and GRB 170817A, *Astrophys. J. Lett.* **848**, L13 (2017).
- [36] M. Punturo *et al.*, The Einstein Telescope: a third-generation gravitational wave observatory, *Class. Quantum Grav.* **27**, 194002 (2010).
- [37] B. P. Abbott *et al.*, Exploring the sensitivity of next generation gravitational wave detectors, *Class. Quantum Grav.* **34**, 044001 (2017).
- [38] P. Amaro-Seoane *et al.*, Astrophysics with the Laser Interferometer Space Antenna, *Living Rev. Relativ.* **26**, 2 (2023).
- [39] A. G. Abac *et al.* (LIGO Scientific, Virgo, and KAGRA), GWTC-4.0: An introduction to version 4.0 of the gravitational-wave transient catalog, *Astrophys. J. Lett.* **995**, L18 (2025).
- [40] E. G. Adelberger, B. R. Heckel, and A. E. Nelson, Tests of the gravitational inverse-square law, *Annu. Rev. Nucl. Part. Sci.* **53**, 77 (2003).
- [41] J. Murata and S. Tanaka, A review of short-range gravity experiments in the LHC era, *Class. Quantum Grav.* **32**, 033001 (2015).
- [42] J. H. Lee *et al.*, New test of the gravitational $1/r^2$ law at separations down to $52 \mu\text{m}$, *Phys. Rev. Lett.* **124**, 101101 (2020).
- [43] D. J. Kapner *et al.*, Tests of the gravitational inverse-square law below the dark-energy length scale, *Phys. Rev. Lett.* **98**, 021101 (2007).
- [44] A. G. Abac *et al.* (LIGO Scientific, Virgo, and KAGRA), Black hole spectroscopy and tests of general relativity with GW250114, *Phys. Rev. Lett.* **136**, 041403 (2026).
- [45] C. Balfagón, Gravitational-wave constraints on causal nonlocal kernels: Data release and analysis code (2026), zenodo.
- [46] W. F. Donoghue, *Monotone Matrix Functions and Analytic Continuation* (Springer, Berlin, 1974).
- [47] R. L. Schilling, R. Song, and Z. Vondraček, *Bernstein Functions: Theory and Applications*, 2nd ed. (De Gruyter, Berlin, 2012).
- [48] C. Bär, N. Ginoux, and F. Pfäffle, *Wave Equations on Lorentzian Manifolds and Quantization* (European Mathematical Society, Zürich, 2007).